Journal of Power Sources 258 (2014) 356–364

Contents lists available at ScienceDirect

Journal of Power Sources

journal homepage: www.elsevier.com/locate/jpowsour

Structural evolution in $LiFePO_4$-based battery materials: *In-situ* and *ex-situ* time-of-flight neutron diffraction study

I.A. Bobrikov [a,*], A.M. Balagurov [a], Chih-Wei Hu [b,c], Chih-Hao Lee [b,c], Tsan-Yao Chen [b], Sangaa Deleg [d], D.A. Balagurov [a]

[a] Frank Laboratory of Neutron Physics, Joint Institute for Nuclear Research, Dubna 141980, Russia
[b] Department of Engineering and System Science, National Tsing Hua University, Hsinchu 30013, Taiwan
[c] National Synchrotron Radiation Research Center, 101 Hsin-Ann Road, Hsinchu Science Park, Hsinchu 30076, Taiwan
[d] Institute of Physics and Technology, Mongolian Academy of Sciences, Ulaanbaatar 210651, Mongolia

HIGHLIGHTS

- Time-of-flight *in-situ* neutron powder diffraction was applied to study commercial Li-ion batteries.
- Comparative study of the behavior of $LiFePO_4$- and V-added $LiFePO_4$-based batteries in charge–discharge cycling was carried out.
- Detailed tracing of the multistage process of Li-insertion into graphite are shown.
- Information on the microstructure of vanadium-added $LiFePO_4$ cathode materials was obtained.

GRAPHICAL ABSTRACT

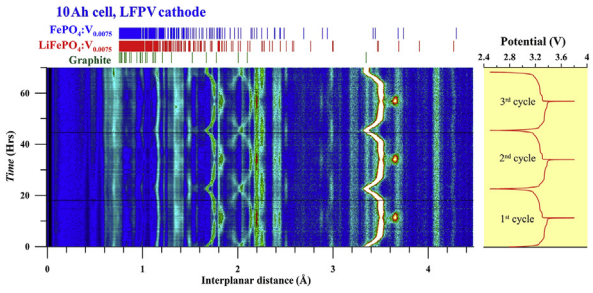

ARTICLE INFO

Article history:
Received 9 December 2013
Received in revised form
4 February 2014
Accepted 15 February 2014
Available online 27 February 2014

Keywords:
Li-ion battery
Time-of-flight neutron diffraction
In-situ studies
Li-intercalation phase
Lithium iron phosphate
Vanadium-addition

ABSTRACT

Neutron diffraction has been used for *in-situ* studying of the charge–discharge processes in commercial lithium batteries with $LiFePO_4$ (LFP) and graphite electrodes. The diffraction data were obtained with time-of-flight diffractometer in the process of three complete charge–discharge cycles performed at a low rate (0.1 C) at room temperature. The experimental data allowed detailed tracing of the multistage process of Li insertion into graphite followed by the formation of several LiC_n phases, as well as the reversible transition of $LiFePO_4 \leftrightarrow FePO_4$. A comparison of the charge–discharge processes in a battery with a pure LFP cathode and LFP containing ~1% of vanadium (LFPV) is made. In the second case, an evidently larger part of the anode material passes into the final LiC_6 state. Analysis of the diffraction patterns of LFP and LFPV powders revealed a marked shrinkage of crystallite size in the LFPV case, which correlates with better electrochemical properties of LFPV compared to LFP.

1. Introduction

Improvement of the performance characteristics of portable power sources requires in-depth understanding of the structural processes occurring in their electrodes. First of all, it is necessary for an adequate quantitative description of the charge transfer between the electrodes. Along with structural rearrangements

* Corresponding author.
E-mail address: bobrikov@nf.jinr.ru (I.A. Bobrikov).

http://dx.doi.org/10.1016/j.jpowsour.2014.02.060
0378-7753/

occurring at the atomic level, changes in the microstructure of the electrode materials during their long-term operation also must be taken into account. For instance, in a recent paper of Harris et al. [1], by using Li-ion half-cell with a graphite electrode it has been shown that diffusion mathematical models not comprising microstructural information can only provide a qualitative description of the charge transfer.

For a long time neutron scattering (first of all, diffraction) is successfully used to study the atomic and magnetic structures of materials applied in batteries and their transformation during electrochemical processes or under environmental conditions changes. In some cases, neutron diffraction allows acquiring data on material microstructure as well. Important for electrode materials studies features of slow neutrons interaction with matter have been already considered in several review articles (see, for instance, Refs. [2,3]). Recent technological advances have allowed using neutron scattering to study the transition phenomena in the electrode materials occurring as a result of their charge or discharge. Moreover, a number of papers have appeared, in which neutron scattering was used for analyzing the behavior of the electrode materials in commercial lithium-ion batteries (as an example, see Refs. [4–6]). Large neutron penetrating depth is one of the most important factors determined success of these works.

$LiFePO_4$ (lithium iron phosphate, LFP) is used as a cathode material in batteries for various devices, including vehicles, but its wider application is limited by the relatively low ionic conductivity. To improve the electrical properties of LFP its doping with vanadium has been suggested and comprehensive structural and electrochemical studies of a new compound $LiFePO_4$:V (LFPV) have been performed. In the literature there is no consensus concerning structural position occupied by vanadium and, consequently, about a mechanism of improving LFPV electrical properties. At first, evidences appeared that there is a greater preference for V to become embedded in phosphorus [7] or iron [8] position. But results obtained in the paper [9] for both compositions LFP and LFPV (up to 5% of V) by several experimental techniques including X-ray and neutron powder diffraction, and X-ray absorption spectroscopy gave evidences for the vanadium substitution at the lithium site. Based on this result the authors suggested the mechanism of the conductivity (by a factor of 40) and capacity (by 14%) enhancement for the V-added compound.

In recent *in-situ* experiments [10] performed by the same group of authors as in Ref. [9] a commercially available battery with LFPV-cathode (added with 0.75% of V) has been studied. The experiments were performed on the WOMBAT diffractometer (OPAL reactor in Australian Nuclear Science and Technology Organisation) with monochromatic neutron beam ($\lambda = 2.4$ Å) and large position-sensitive detector ($1.35 \leq d_{hkl} \leq 6.28$ Å range). In several completed charge–discharge cycles, gradual transformation of $LiFePO_4$:V into its delithiated form ($FePO_4$:V) and evolution of structural phases of the anode Li_xC_6 with $0 < x \leq 1$ were observed. It has been demonstrated, in particular, that in the LFPV-cathode battery the $LiFePO_4$:V ↔ $FePO_4$:V transformation occur synchronously with the change of the battery charge.

In the following, we report the results of *in-situ* neutron diffraction experiments with Li-ion batteries with pristine and V-added LFP-cathodes. The main objective of the study was a comparative analysis of the behavior of LFP and LFPV batteries in charge–discharge cycling. The experiments were performed at a pulsed neutron source using the time-of-flight (TOF) technique. An important advantage of the TOF method is the possibility to work at the fixed scattering geometry, which allows selecting the optimal battery orientation relative to the directions of the incident and scattered neutron beams and, thus, minimizing the difficulties associated with complex internal structure of a battery. Neutron *in-situ* studies of commercial batteries using TOF technique is just beginning (see, e.g., [11,12]), so another challenge was the development of an appropriate experimental arrangement and software for data acquisition and analysis. One of the most important results of these experiments is the finding that in the LFPV case, an evidently larger part of the anode material passes into the final LiC_6 state.

Besides *in-situ* experiments, neutron powder diffraction patterns of $LiFePO_4$:V (up to 5% of V) were measured, based on which certain conclusion about the evolution of crystalline microstructure with increasing vanadium concentration was made. In particular, a marked shrinkage of crystallite size was revealed that correlates with better electrochemical properties of LFPV compared to LFP.

2. Experimental part

For the experiments we used two commercial batteries with the following sizes: $3 \times 100 \times 136$ mm (battery №1, a nominal capacity ~2 Ah) and $8.2 \times 128 \times 155$ mm (battery №2, a nominal capacity ~10 Ah) (Fig. 1), which are produced by Advanced Lithium Electrochemistry Co. Ltd. (ALEEES), Taiwan. Both batteries contained graphite anode with real specific capacity 330 mAh g^{-1}, electrolyte $LiPF_6$ mixed with ethylene- and dimethyl-carbonates, polypropylene/polyethylene separator, copper (for the anode) and aluminum (for the cathode) current collectors. As a cathode battery №1 includes carbon coated $LiFePO_4$, in the second battery the carbon coated vanadium added material was used, i.e. $LiFePO_4$:V_δ, $\delta = 0.75\%$. These both materials have been investigated in paper [9], where it was determined, in particular, that the specific capacity is 138 mAh g^{-1} for LFP and 155 mAh g^{-1} for LFPV. A proportion between amount of anode and cathode materials was kept constant for both batteries. As it is mentioned in Introduction, in Ref. [10] the battery similar to our №2 has been already studied previously. The synthesis procedure of LFP and LFPV cathode materials is described in Ref. [9]. For charge–discharge cycling we used a galvanostat KIKUSUI PFX2011. Before diffraction experiment batteries №1 and №2 had 5 and 20 full charge–discharge cycles, correspondingly.

The neutron diffraction experiments were performed at the HRFD instrument (High Resolution Fourier Diffractometer) [13], which provides the possibility to work in two modes of diffraction data acquisition: high resolution in reciprocal space (using the Fourier chopper and correlation electronics, $\Delta d/d \approx 0.001$, where d is interplanar distance) and high luminosity (conventional TOF-method, $\Delta d/d \approx 0.01$). The geometry of the experiment is shown in Fig. 2, which demonstrates that the registration of the diffraction

Fig. 1. Li-ion battery (10 Ah) with current terminals through which it was charged and discharged. Its dimensions are $8.2 \times 128 \times 155$ mm.

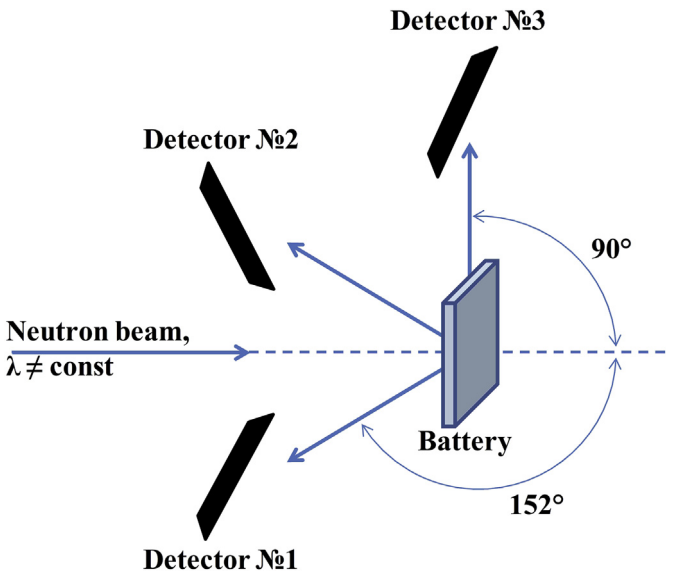

Fig. 2. Schematic illustration of the experimental arrangement. The incoming white beam is formed by a neutron guide, three detectors are placed at average scattering angles of $2\theta = \pm 152^\circ$ and 90°. To improve resolution the time focusing conditions are used, this is why the detector planes are rotated relative to the line connecting the center of the sample and the detector.

patterns was carried out by three detectors placed at $2\theta = \pm 152^\circ$ and 90°. The covered d-spacing range is 0.7–3.7 Å for back-scattering detectors and 1–5 Å for the 90°-detectors. Neutron beam impinges on 10×60 mm^2 of the whole battery surface.

Before *in-situ* experiments with the batteries, measurements of neutron diffraction patterns of $LiFePO_4$ and $LiFePO_4$:V_δ powders, $\delta = 0.75$, 2 and 5% (Fig. 3), at several temperatures have been performed. It allowed refining the structural characteristics of the materials used for manufacturing battery cathodes. Naturally, the quality of the diffraction patterns measured from the battery assembly was not too good due to high incoherent background of the hydrogen component of the additional battery materials – the separator and the electrolyte. However, it was sufficient (Fig. 4) to perform identification of structural phases, to evaluate their parameters and quantity. The diffraction peaks of the aluminum shell of the studied power sources and of the current collectors were weak and did not affect the diffraction data processing.

During the *in-situ* experiments both №1 and №2 batteries were operated between 2.5 and 3.8 V at a constant current of 0.2 A and 1 A corresponds to 0.1 C, where C is their full capacity. I.e. batteries charging or discharging lasted about 10 h. We found that the real capacity of the battery №1 at cutoff potential is 2070 mAh that coincides well with the nominal value 2 Ah. For the battery №2 real capacity is 11,090 mAh at the same cutoff potential that 10% higher that the nominal 10 Ah. The diffraction data were collected continuously in a high intensity mode of HRFD with the acquisition time per one diffraction pattern of 10 min. Battery №2 was additionally studied at the rate of 1 C, for which 8 full charge–discharge cycles were performed. In this case the acquisition time of one diffraction pattern was 2.5 min. After each charge or discharge a 10-min pause was held in order to damp the inertial processes inside the batteries. From time to time the high-resolution mode was used to analyze the phase composition and to obtain precise structural data on the anode and cathode materials in the batteries in a steady state. For example, at 50% battery charge in the diffraction pattern there are peaks corresponding to six structural phases.

The analysis of the diffraction patterns by Rietveld method was performed using software packages MRIA [14] and FullProf [15]. For the calculations we use the following crystallographic data on the basic structural phases of the batteries electrodes:

$LiFePO_4$ *Pnma*, $a = 10.337$ Å, $b = 6.011$ Å, $c = 4.695$ Å (see Ref. [16]);
$FePO_4$ *Pnma*, $a = 9.759$ Å, $b = 5.752$ Å, $c = 4.756$ Å (see Ref. [16]);
Graphite $P6_3/mmc$, $a = b = 2.458$ Å, $c = 6.724$ Å (our data);
$LiC_{n>18}$ $P6/mmm$, $a = b \approx 7.37$ Å, $10\ \text{Å} \le c \le 27.2$ Å (see Ref. [17]);
LiC_{18} $P6/mmm$, $a = b \approx 7.37$ Å, $c \approx 7.047$ Å (see Ref. [18])
LiC_{12} $P6/mmm$, $a = b = 4.290$ Å, $c = 7.047$ Å (see Ref. [11]);
LiC_6 $P6/mmm$, $a = b = 4.307$ Å, $c = 3.680$ Å (see Ref. [11]);

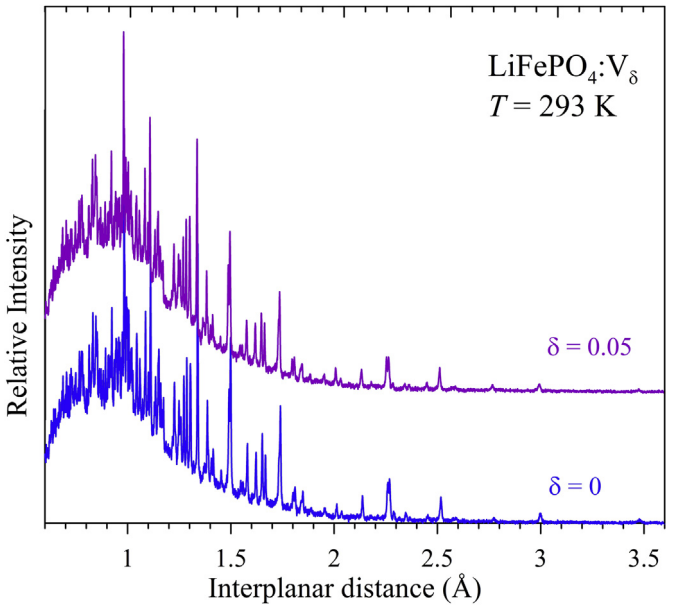

Fig. 3. Diffraction patterns (non-normalized to the incident neutron flux) for $LiFePO_4$ and $LiFePO_4$:V_δ powders measured at HRFD with back-scattering detectors in high-resolution mode ($\Delta d/d \approx 0.001$).

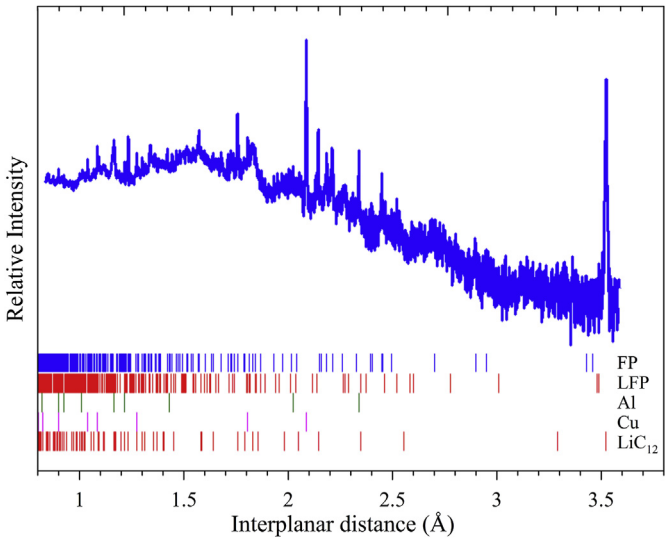

Fig. 4. Diffraction pattern (normalized to the incident neutron flux) for battery №1 at 50% state of charge (SOC) measured at HRFD at room temperature in high-resolution mode ($\Delta d/d \approx 0.001$). Anode material is in the LiC_{12} phase. Positions of diffraction lines for several main phases are indicated.

3. Experimental results

The diffraction patterns of the materials used for manufacturing battery cathodes (shown in Fig. 3) were processed by a structural model from Ref. [16]. The results of data processing for pristine LFP (Fig. 5) and the V-added LFP are in good agreement with the model – the coordinates of the atoms almost coincide for all δ. Our attempts to determine which of the cations is substituted with vanadium when doping $LiFePO_4$ did not lead to any definite result – the refinement of $LiFePO_4$:V_δ structure with $\delta = 2\%$ and 5% indicated emergence of a number of vacancies in all possible positions: Li, Fe, and P. However, due to strong correlations between atomic occupancies and thermal factors the accuracy of this result is not high. The lengths of interatomic distances in the LFP and LFPV structures coincide to an accuracy of ~0.01 Å, which also makes it impossible to specify the position of substitution. In the unit cell parameters, which are the most accurately determined by the diffraction data values, marked changes are observed at least at the 5% of vanadium adding. There is some difference in absolute values of the lattice parameters measured at various instruments depending mainly on calibration of a diffractometer. But comparison of the relative changes shows a clear tendency (Fig. 6). The same tendency – increase of c and decrease of a and b parameters – was found in X-ray experiment [7] for V content up to 15%. This, apparently, is the certain evidence of vanadium insertion into the structure.

According to [16] LFP is a collinear antiferromagnet (AFM) with $k = (0,0,0)$ and $T_N = 52$ K. The relative change in the intensity of a diffraction peak with a large magnetic contribution is shown in Fig. 7, from which it can be deduced that in respect of magnetism the material used for manufacturing cathodes does not differ from the standard $LiFePO_4$ powder. The same dependence was obtained for LFPV, i.e. the influence of small amounts of vanadium on the AFM transition point is insignificant.

The diffraction data set (in 2D representation) acquired in *in-situ* mode in the process of three charge–discharge cycles (each cycle lasting about 22 h) is shown in Fig. 8. The vertical axis shows astronomical time (in hours), the horizontal axis corresponds to the interplanar distance (in Å). At the top the positions of the diffraction peaks for the three main structural phases of LFP-battery, the set of which provides their unique characterization, are given. The most intense lines in the range of 3.2–3.7 Å (the so-called "anode window") are associated with a graphite electrode. In the range of 2.2–3.2 Å ("cathode window") several intense peaks of $LiFePO_4$/$FePO_4$ phases are observed.

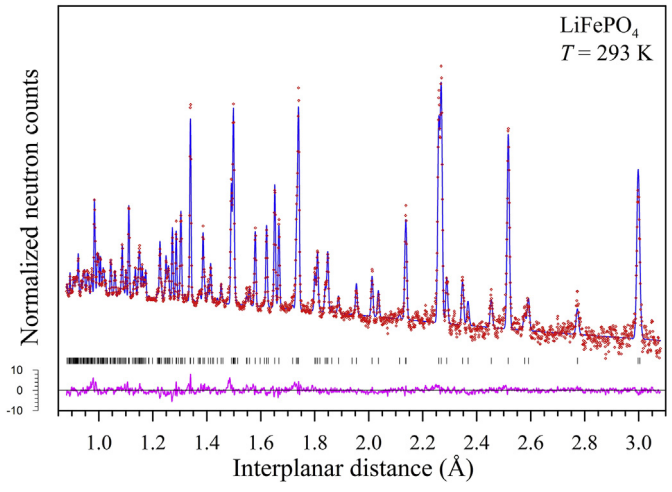

Fig. 5. Diffraction pattern of $LiFePO_4$:V_δ ($\delta = 0.05$) powder measured at HRFD at 293 K in high-resolution mode and processed using Rietveld method. Vertical tikes indicate the calculated positions of diffraction peaks. Difference function (at the bottom) is normalized to statistical error.

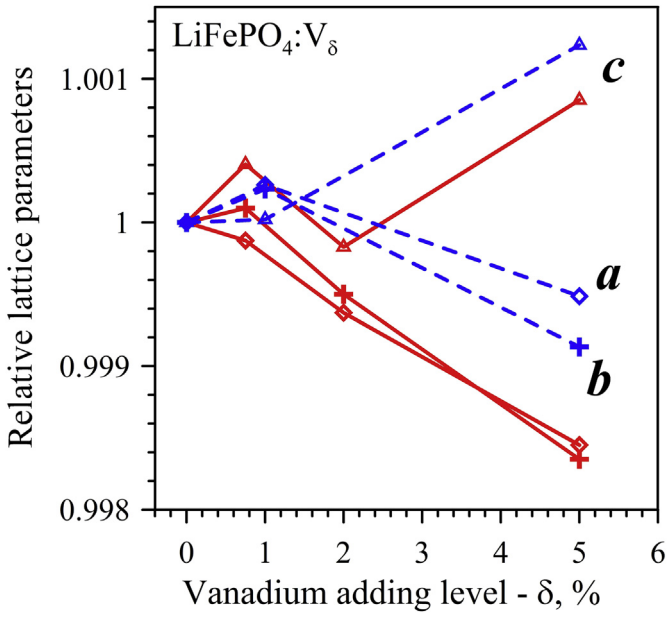

Fig. 6. Relative changes in parameters of the $LiFePO_4$:V_δ orthorhombic cell at different vanadium content. Two sets of experimental points are shown: neutron data measured at HRFD (red points, solid lines), X-ray data from Ref. [9] (blue points, dashed lines). Statistical errors are smaller than symbol size. (For interpretation of the references to color in this figure legend, the reader is referred to the web version of this article.)

Evolution of the intense lines in the "anode window" (3D view in Fig. 9) is associated with the transitions between the LiC_n phases, where $n \geq 6$ (or as it is stated in certain papers, Li_xC_6, $x \leq 1$), which are formed in the transitions of lithium from $LiFePO_4$ into graphite and *vice versa*. Initial, fully discharged state of the battery is characterized by the (002) diffraction peak of pure graphite with $d \approx 3.35$ Å (Fig.10). A fully charged battery demonstrates a LiC_6 phase (a detached spot at $d \approx 3.67$ Å), which under normal

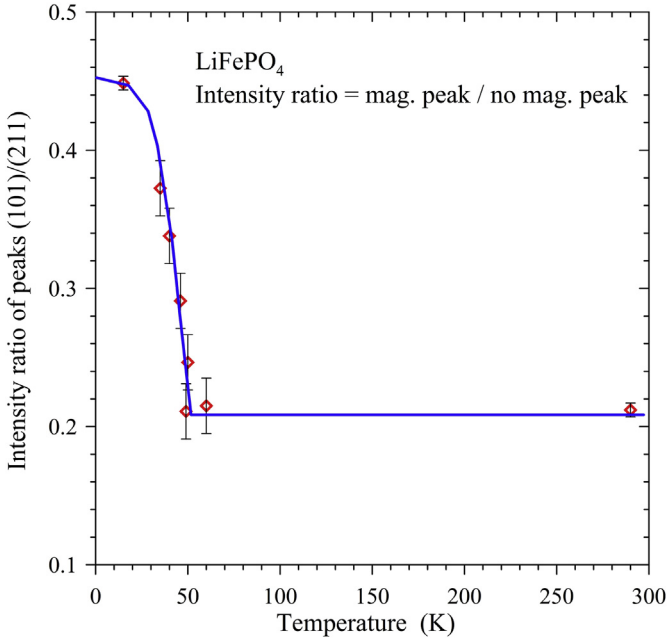

Fig. 7. Temperature dependence of the magnetic contribution to the (101) peak intensity. Transition to a collinear antiferromagnetic phase occurs at $T_N \approx 50$ K.

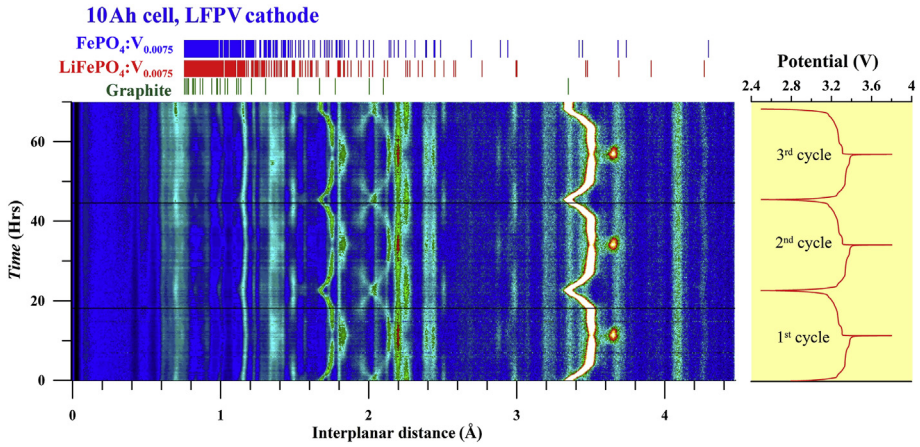

Fig. 8. Evolution of diffraction patterns of a vanadium-doped LFP-battery (№2) produced in the course of three complete charge–discharge cycles at the rate of 0.1 C. Vertical lines at the top indicate positions of diffraction peaks of three main structural phases in their initial state.

conditions is the phase of the maximum possible insertion of lithium into graphite (see, for example, the review [19]). Intermediate phase LiC_{12} ($d \approx 3.51$ Å) is clearly visible at 50% battery charge.

The structural phase diagram of Li-intercalated graphite phases has been described in detail in literature [17,20,21] and our results are in good agreement with it. In particular, the data shown in Figs. 8–10 demonstrate that at the initial stage the (00*l*) diffraction peaks (reflection from planes, which are perpendicular to the hexagonal axis) gradually shift toward larger *d*-spacings. This shift is associated with successive emergence of lithium-intercalated LiC_n phases. The literature contains information on the phases with *n* in the range of 6–72 (see, for example, [17]). Accumulation of lithium results in a gradual increase in the distance between graphite layers, up to the emergence of the LiC_{18} phase. With a further increase in the concentration of lithium ions the transition of LiC_{18} into LiC_{12} mainly occurs due to redistribution of lithium in the basal planes of the structure. In this case the distance between the graphite layers varies insignificantly, which is manifested as the constancy of the peak position with $d \approx 3.51$ Å in the range of 45–80% state of charge (SOC). The similar behavior of the diffraction peak was observed in Ref. [21] for the concentrations of 0.25–0.5 Li atoms per carbon atom, which corresponds to the phases LiC_{24}–LiC_{12}, as well as in recent neutron diffraction papers [10,11].

In the formation of the final phase LiC_6 corresponding to a fully charged condition, the distance between the graphite layers is changed immediately to ~0.2 Å, which is manifested as the step-like appearance of the diffraction peak at $d \approx 3.67$ Å, and the phase LiC_{12} does not vanish completely. That is possibly connected with the significantly excessive general capacity of used graphite relative to the cathode capacity in these cells. Moreover, a part of the graphite anode material remains in its initial state, which is indicated by a bright non-vanishing band at $d \approx 3.35$ Å in Fig. 8.

More detailed information on the successive formation of various LiC_n phases and their content in the volume of the anode is presented in Figs. 11 and 12. The first one illustrates the change in intensity over time (SOC ramping) at fixed *d*-spacings corresponding to the position of maximum of the diffraction peak (00*l*) from LiC_n phases. Fig. 12 shows the relative changes of the diffraction peaks intensities belonging to different LiC_n phases over time. From these graphs one can estimate the rate of change of the content of a particular phase in the bulk of material and the differences in the processes in LFP and LFPV-batteries. In particular, in case of LFPV-cathode a considerably greater part of the anode material passes into LiC_6 state; relative growth is about

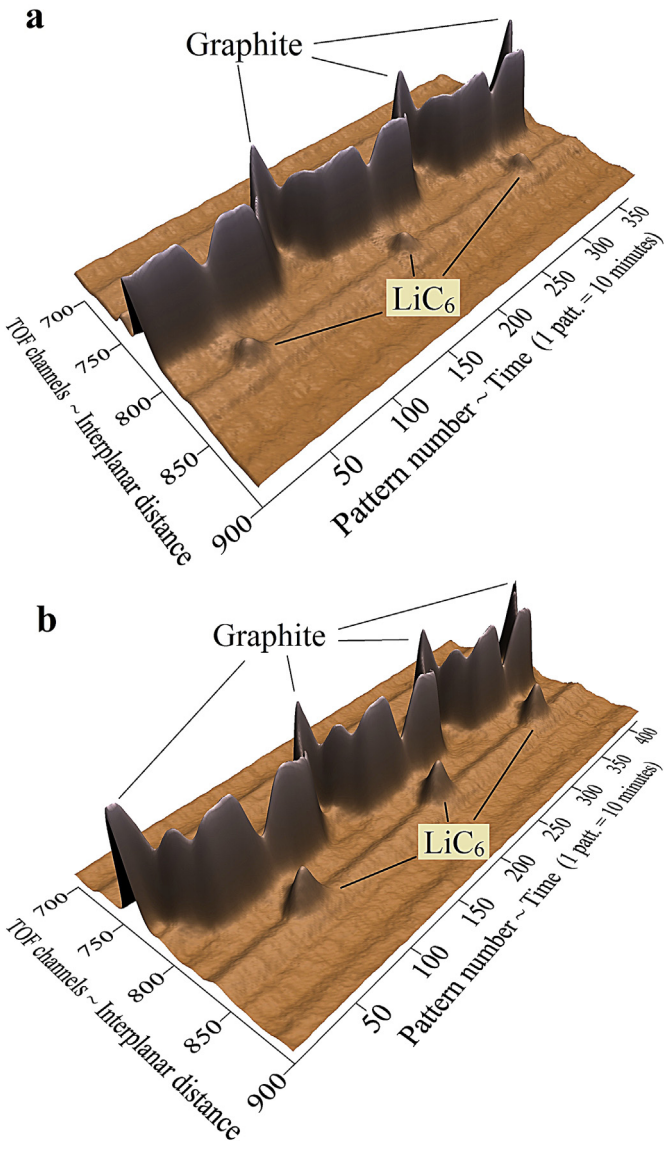

Fig. 9. 3D visualization of diffraction peak evolution from graphite in the "anode-window" region for three charge–discharge cycles for battery №1 (a) and №2 (b). Abrupt emergence of LiC_6 phase is especially evident for battery №2, in which cathode material is doped with vanadium oxide.

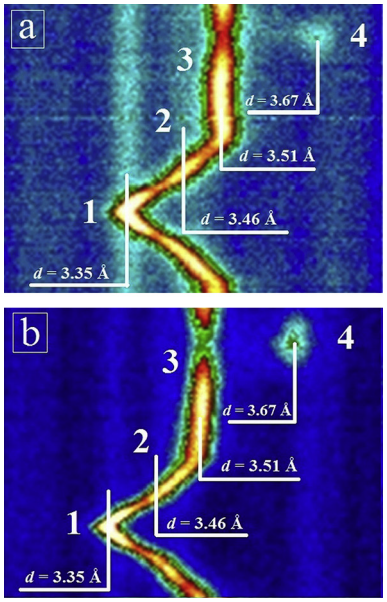

Fig. 10. Enlarged (from Fig. 8) 2D diffraction pattern region characterizing structural processes in LFP-battery anode. Initial state of the anode – graphite without lithium (1, d = 3.35 Å), and sequentially emerging phases $LiC_{\sim 27}$ (2, d = 3.46 Å), LiC_{18}, LiC_{12} (3, d = 3.51 Å) and LiC_6 (4, d = 3.67 Å) for battery №1 (a) and №2 (b) are specified.

10%. Just this effect is responsible for higher specific capacity of the LFPV battery. In addition, it is clearly seen from Fig. 12 that at the end of the charge cycle the anode material is in multiphase state.

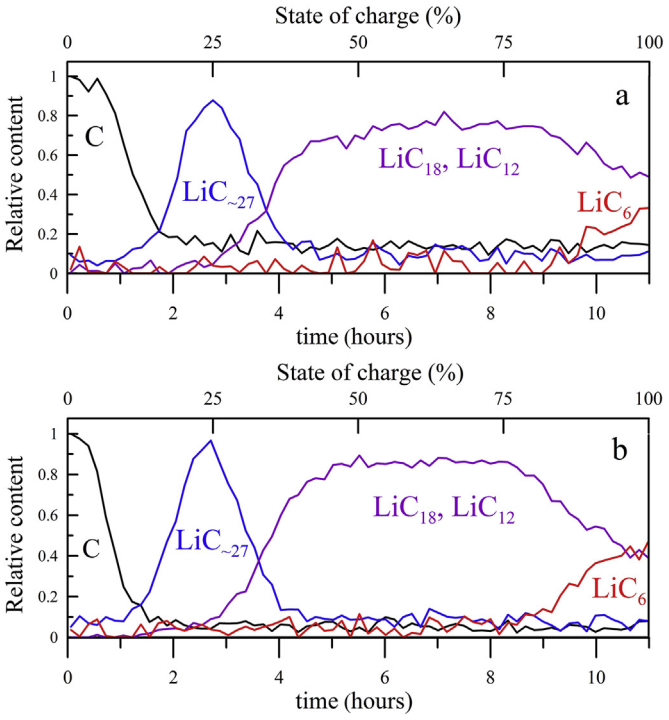

Fig. 12. Content of different LiC_n phases of battery №1 (a) and 2 (b) in course of one charge cycle as a function of time (lower scale) or SOC (upper scale) recovered from relative changes in intensity of corresponding diffraction peaks. It is seen that at the end of charge cycle the anode material is non-uniform in its lithium content state and that in case of the LFPV-cathode a larger part of the anode volume passes into LiC_6 phase.

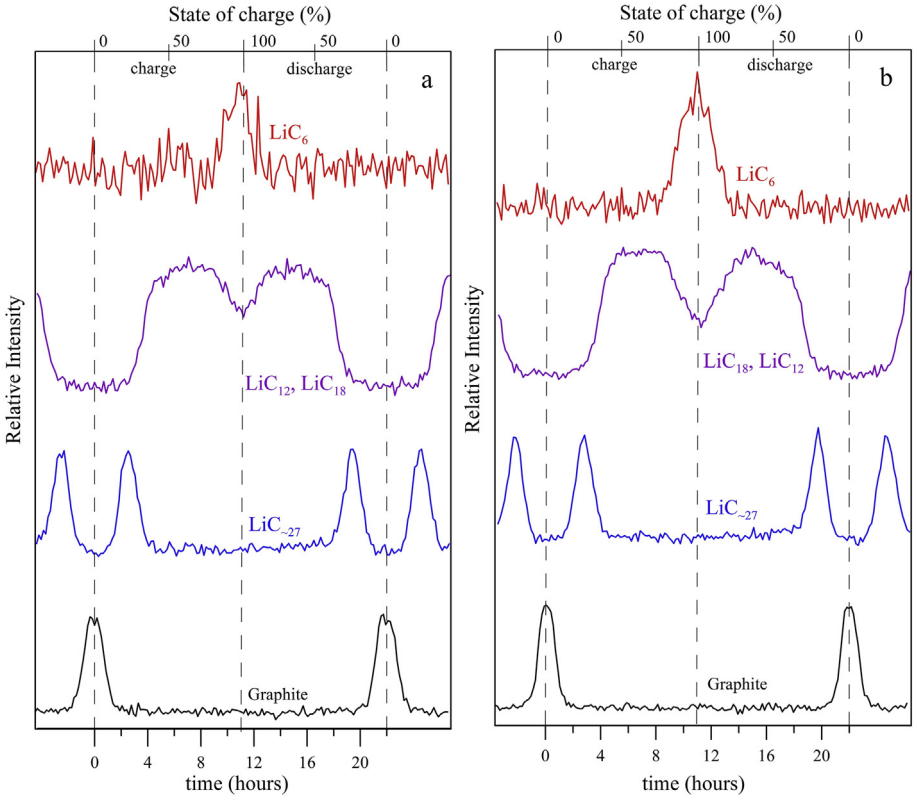

Fig. 11. Changes in intensity of diffraction peaks of graphite and LiC_n phases depending on the battery №. 1 (a) and 2 (b) charge states in course of one charge–discharge cycle. Horizontal axis shows time in hours. Intensities are taken at fixed values of d-spacings for pure graphite d_{002} = 3.35 Å, $LiC_{\sim 27}$ – d_{003} = 3.46 Å, LiC_{18}, LiC_{12} – d_{002} = 3.51 Å and LiC_6 – d_{001} = 3.67 Å.

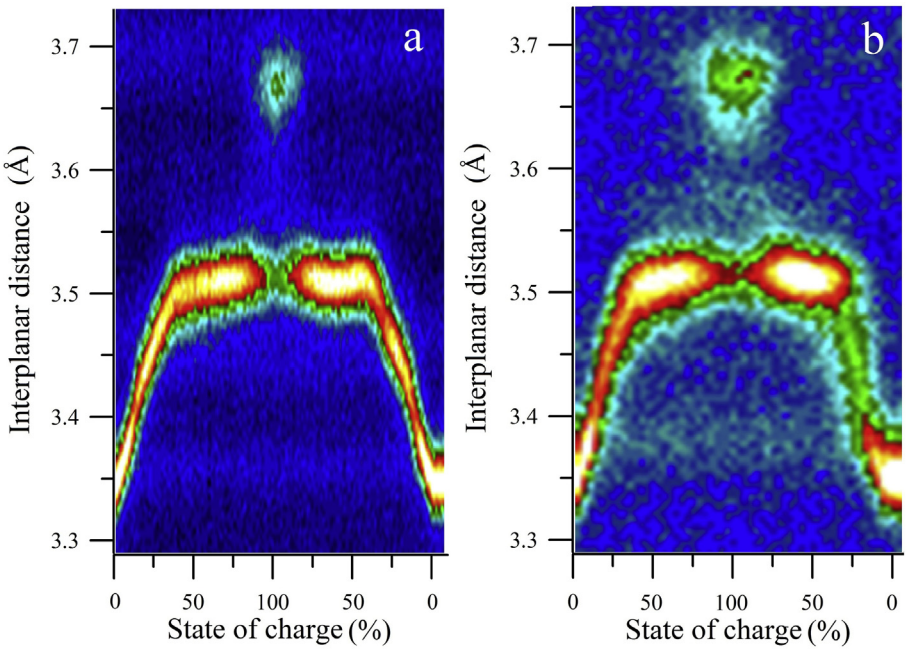

Fig. 13. Comparison of the "anode" region of diffraction patterns obtained from battery №2 at cycling rates 0.1 C (a) and 1 C (b). Differences between them are clearly visible in the region corresponding to the battery discharge.

From the above-mentioned changes in the intensity of the diffraction peaks over time, it follows that at the charge–discharge rate of 0.1 C the emergence and vanishing of LiC_n phases is completely symmetrical with respect to the point of full battery charge. However, in the experiment with battery №2 at the cycling rate of 1 C asymmetry in these processes was observed, which is clearly visible in Fig. 13. At a high rate the battery discharging is more surge, the intermediate states between the LiC_{12}/LiC_{18} phases (maximum at $d = 3.51$ Å) and graphite are not traced as clearly as in the charging process.

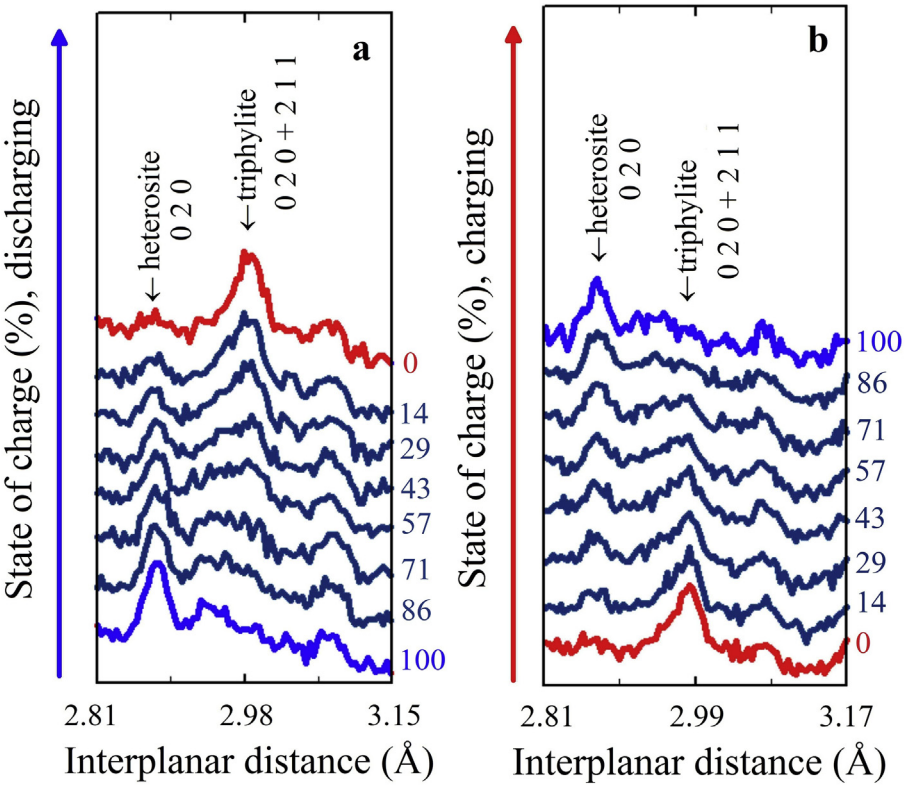

Fig. 14. Typical region of diffraction patterns from battery №1 comprising diffraction peaks of $LiFePO_4$ (triphylite) and $FePO_4$ (heterosite). They were measured in *in-situ* mode during discharging (a) and charging (b) of the battery. Measurement time for each pattern was 10 min. Numbers on the right indicate battery charge state (in %).

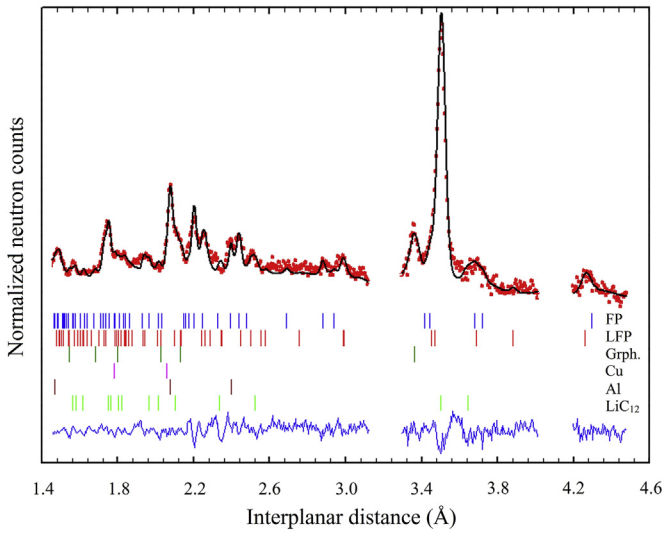

Fig. 15. An example of Rietveld neutron powder diffraction pattern for a half-charged battery №1 (~45% SOC) measured in 30 min. Experimental points, calculated profile and difference curve (at the bottom) are given. Vertical tikes indicate calculated d_{hkl} for six phases: $FePO_4$, $LiFePO_4$, pure graphite, Cu, Al and LiC_{12} (from top to bottom). Parts of pattern containing broad peaks of separator components are removed.

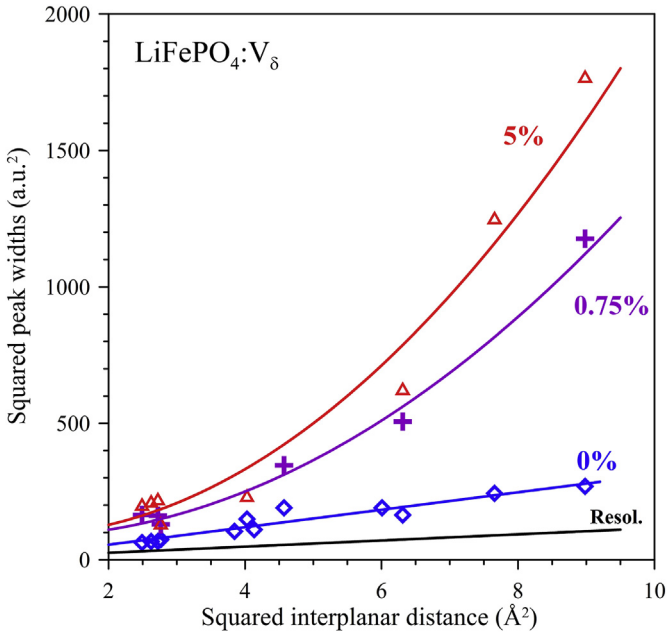

Fig. 17. Dependences of diffraction peak widths on d-spacing. For the parent $LiFePO_4$ ($\delta = 0$) a linear dependence is measured, whereas for $\delta > 0$ the dependence is parabolic due to a small size of coherent scattering domains. Bottom (black) line corresponds to resolution function of diffractometer measured with a standard sample.

Fig. 14 illustrates changes in the intensities of the diffraction peaks in the region of the "cathode window" showing the vanishing of $LiFePO_4$ and appearance of $FePO_4$ (and *vice versa*) during the battery charging (discharging). The analysis of the intensities of the diffraction peaks allows determining the relative content of these phases depending on the degree of battery charge with an uncertainty at a few percent level. For pure LFP the transition process $LiFePO_4 \rightarrow xFePO_4 + (1 - x)LiFePO_4$ and back has already been studied using X-ray diffraction [22], and it has been demonstrated that the content of the phases varies linearly over time. Similar results were obtained by neutron diffraction for pure LFP [23] and LFP doped with 1% of vanadium [10]. According to our data, there is a slight asymmetry in the change of the $LiFePO_4$ and $FePO_4$ phase content and the degree of battery charge. Thus, for the discharged batteries the content of $FePO_4$ and $LiFePO_4$ is 0.43/0.57 and 0.37/0.63 for batteries №1 and №2, respectively. For the half-discharged cells its values are 0.66/0.34 and 0.69/0.31. The deviation of the content of $FePO_4$ and $LiFePO_4$ phases from the expected proportions 0/1 at 0% SOC and 0.5/0.5 at 50% SOC is presumably related to the irreversible loss by $LiFePO_4$ phase of large number of Li atoms used for formation of solid electrolyte interphase (SEI) and weak lithium saturation of graphite (that is not detected by neutron diffraction but it is seen by potential presence between electrodes). For the full-charged batteries (cutoff voltage was 3.8 V in both cases) the content of $FePO_4$ and $LiFePO_4$ is 0.93/0.07 and 1/0 for batteries №1 and №2. It means that common LFP cathode has small part of initial phase at full charged condition of battery but cathode with vanadium addition has only one phase – $FePO_4$. Uncertainties for the phase content are large (~10%) but tendency is clear: LFPV works effectively than LFP.

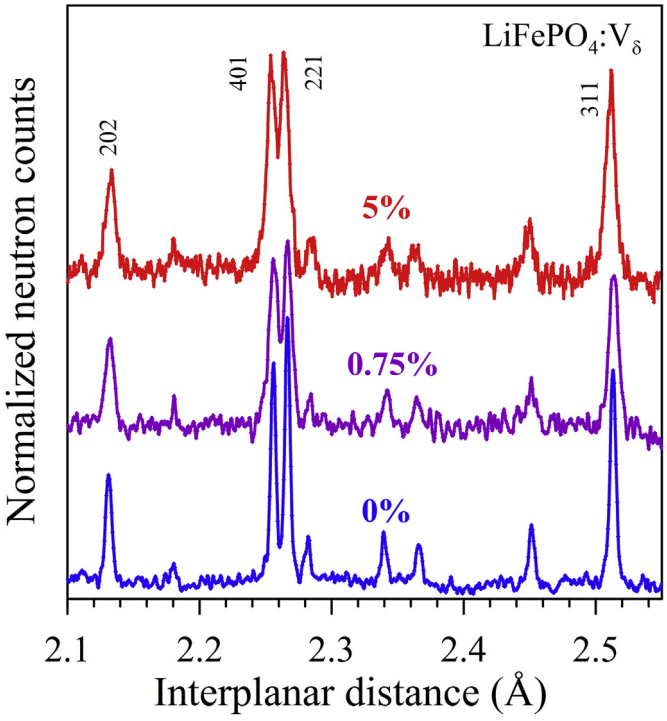

Fig. 16. Portion of a diffraction pattern for $LiFePO_4$ with different content of vanadium (numbers near the curves) measured in high-resolution mode. Width of peaks and incoherent background increase with rising vanadium content. Miller indices are given for the most intense peaks.

These results were obtained from the analysis of individual diffraction patterns using the Rietveld method. The illustration of processing of a pattern measured over 30 min at the high intensity mode of the diffractometer, with a half-charged battery (~50% SOC) and containing 6 structural phases is shown in Fig. 15.

High-resolution neutron diffraction provides opportunity to obtain information on the microstructural parameters of the crystalline substance – average size of coherently scattered domains and the microstress level, i.e. to estimate its defectiveness. It was obtained from the analysis of the Bragg peak broadening (anisotropic in general) as a function of d_{hkl}-spacing. The functional dependence of microstrain and size effects on d_{hkl} is different, which makes it possible to separate them. Fig. 16 shows a typical region of the $LiFePO_4$:V_δ diffraction pattern with different content

of vanadium, from which it can be observed that the peaks broaden with increasing δ. The dependencies of the diffraction full-width at half-maximum, W, on the d-spacing for the initial LFP and LFPV doped with 0.75% and 5% of vanadium are given in Fig. 17. For the HRFD diffractometer the $W^2(d^2)$ dependence for a powder consisting of large crystallites (>3000 Å) and without microstresses is seen as a linear (resolution) function (lower line in Fig. 17). In the presence of microstresses the line slope increases, and in the presence of size effect the dependence becomes quadratic. From the graphs it is seen that there is a small microstress level in LFP crystallites ($\delta = 0$) and no size effect, whereas in LFPV a significant broadening of the diffraction peaks is due to the reduction of the size of domains to ~600 Å at $\delta = 0.75\%$ and down to ~400 Å at $\delta = 5\%$.

4. Discussion and conclusions

Neutron diffraction experiments with LFP- and LFPV-batteries carried out at the HRFD facility at the IBR-2 pulse reactor have allowed real-time monitoring of transition processes occurring in their electrodes during charge–discharge cycles. The obtained data allow us to reliably identify emerging structural phases and quantitatively analyze the kinetics of phase transformations in the anode and cathode. An important feature of the HRFD is the possibility to switch between two different modes of operation – high intensity and high resolution – without changing the experiment geometry. High-intensity mode was used for *in-situ real-time* data accumulation with a reasonable time (every 10 min) for statistics. High-resolution mode was used for data accumulation on the stationary states of the batteries, which allowed for the reliable identification and analysis of emerging structural phases. It can be asserted that the TOF diffraction at the HRFD is a promising technique for studying the materials that make up Li-batteries, as well as transition processes in them.

The acquired diffraction data allowed detailed tracing of the multistage process of Li insertion into graphite followed by the formation of several LiC_n phases, at first accompanied by a gradual increase in the distance between the carbon layers, and then by the redistribution of lithium in the basal planes of graphite structure. Formation at the charge of the final LiC_6 phase is easily detected by a step-like emergence of a diffraction peak at $d \approx 3.67$ Å. In the state of a full charge LiC_6 phase takes about 50% of the initial volume of the graphite electrode, the remaining volume is occupied by phases not fully saturated with lithium (mainly LiC_{12}). In the 10 Ah battery based on the LFPV-cathode a ~10% larger part of the anode material passes into LiC_6 state if compared with the LFP battery.

Comparison of phase transformations in the anode at different charge–discharge rates has shown that at the rate of 0.1 C clearly marked peaks of intensity corresponding to intermediate states between graphite and (LiC_{12}/LiC_{18}) phases are observed, and the emergence and vanishing of the LiC_n phase is completely symmetrical with respect to the point of full battery charge. On the contrary, when cycling at the rate of 1 C, intermediate states during charging and especially discharging are not traced in the form of clear intensity maxima of the diffraction peaks.

Lower intensity of the diffraction peaks from the cathode material and its more complex crystal structure do not allow tracing structural changes in the cathode in as much detail as in the anode. Nevertheless, $LiFePO_4 \leftrightarrow FePO_4$ transitions are clearly seen and quantifiable. The Rietveld analysis of diffraction patterns obtained for particular points of SOC for both batteries revealed that noticeable larger volume part of LFPV cathode takes part in the battery operation in comparison with pure LFP. This correlates with larger amount of the LiC_6 phase in LFPV battery in comparison with LFP one. These results correlate also with greater real capacity of battery №1 (~11 Ah) than its nominal value (10 Ah).

High resolution of the HRFD allowed analyzing the changes in the cathode material microstructure when inserted with vanadium. In pure $LiFePO_4$ a slight broadening of the diffraction peaks is observed due to the presence of a certain microstress level. In powders $LiFePO_4$:V_δ at $\delta = 0.75\%$, and especially at $\delta = 5\%$ the diffraction peaks are strongly broadened due to size effect. It means that when inserting vanadium into the $LiFePO_4$ structure, a significant (from a few thousand to about 400 Å) decrease of crystal long-range order occurs. This effect can be interpreted as a considerable increase in the density of defects, which correlates with better electrochemical LFPV properties if compared to LFP.

Acknowledgments

The authors are grateful to V.G. Simkin for substantial help in carrying out the experiments at the HRFD, to Prof. E.V. Antipov and Dr. O.A. Drozhzhin for fruitful discussion of the results. The work was supported in part by RFBR grants (12-02-92200-Mong-a, 12-02-00686-a), as well as by JINR grant №13-401-01.

References

[1] S.J. Harris, A. Timmons, D.R. Baker, C. Monroe, Chem. Phys. Lett. 485 (2010) 265–274.
[2] H. Wang, R.G. Downing, J.A. Dura, D.S. Hussey, ACS Symp. Ser. 1096 (6) (2012) 91–106.
[3] N. Sharma, V.K. Peterson, J. Solid State Electrochem. 16 (2012) 1849–1856.
[4] M.A. Rodriguez, D. Ingersoll, S.C. Vogel, D.J. Williams, Electrochem. Solid-State Lett. 7 (2004) A8–A10.
[5] N. Sharma, V.K. Peterson, M.M. Elcombe, M. Avdeev, A.J. Studer, N. Blagojevic, R. Yusoff, N. Kamarulzaman, J. Power Sources 195 (2010) 8258–8266.
[6] A. Senyshyn, M.J. Mühlbauer, K. Nikolowski, T. Pirling, H. Ehrenberg, J. Power Sources 203 (2012) 126–129.
[7] J. Hong, C.S. Wang, X. Chen, S. Upreti, M.S. Whittingham, Electrochem. Solid-State Lett. 12 (2009) A33–A38.
[8] J. Ma, B. Li, H. Du, C. Xu, F. Kang, J. Electrochem. Soc. 158 (2011) A26–A32.
[9] C.-Y. Chiang, H.-C. Su, P.-J. Wu, H.-J. Liu, C.-W. Hu, N. Sharma, V.K. Peterson, H.-W. Hsieh, Y.-F. Lin, W.-C. Chou, C.-H. Lee, J.-F. Lee, B.-Y. Shew, J. Phys. Chem. C 116 (2012) 24424–24429.
[10] C.-W. Hu, N. Sharma, C.-Y. Chiang, H.-C. Su, V.K. Peterson, H.-W. Hsieh, Y.-F. Lin, W.-C. Chou, B.-Y. Shew, C.-H. Lee, J. Power Sources 244 (2013) 158–163.
[11] X.-L. Wang, Ke An, Lu Cai, Z. Feng, S.E. Nagler, C. Daniel, K.J. Rhodes, A.D. Stoica, H.D. Skorpenske, C. Liang, W. Zhang, J. Kim, Y. Qi, S.J. Harris, Nat. Sci. Rep. 2 (747) (2012) 1–6.
[12] H. Liu, C.R. Fell, Ke An, Lu Cai, Y.S. Meng, J. Power Sources 240 (2013) 772–778.
[13] A.M. Balagurov, Neutron News 16 (2005) 8–12.
[14] V.B. Zlokazov, V.V. Chernyshev, J. Appl. Crystallogr. 25 (1992) 447–451.
[15] J. Rodríguez-Carvajal, Phys. B 192 (1993) 55.
[16] G. Rousse, J. Rodriguez-Carvajal, S. Patoux, C. Masquelier, Chem. Mater. 15 (2003) 4082–4090.
[17] T. Ohzuku, Y. Iwakoshi, K. Sawai, J. Electrochem. Soc. 140 (9) (1993) 2490–2497.
[18] A. Hérold, Intercalated Layer. Mater. 6 (1979) 323–421.
[19] M. Winter, J.O. Besenhard, M.E. Spahr, P. Novak, Adv. Mater. 10 (1998) 725–763.
[20] A. Senyshyn, O. Dolotko, M.J. Mühlbauer, K. Nikolowski, H. Fuess, H. Ehrenberg, J. Electrochem. Soc. 160 (5) (2013) A3198–A3205.
[21] J.R. Dahn, Phys. Rev. B 44 (1991) 9170–9177.
[22] A.S. Andersson, B. Kalska, L. Häggström, J.O. Thomas, Solid State Ionics 130 (2000) 41–52.
[23] M. Roberts, J.J. Biendicho, S. Hull, P. Beran, T. Gustafsson, G. Svensson, K. Edström, J. Power Sources 226 (2013) 249–255.